Turkish Journal of Electrical Engineering & Computer Sciences

http://journals.tubitak.gov.tr/elektrik/

Research Article

Turk J Elec Eng & Comp Sci
(2015) 23: 2017 – 2029

doi:10.3906/elk-1404-256

New three-dimensional space vector pulse width modulation of PV-AF system based on the ghγ coordinate system

Juan ZHOU[1,*], **Malong LIU**[2], **Chen WEI**[1], **Chaoxu GAO**[1], **Xiaojie WU**[1]
[1]School of Information and Electrical Engineering, China University of Mining and Technology, Xuzhou, P.R. China
[2]Henan Electric Power Survey & Design Institute, Zhengzhou, P.R. China

Received: 14.04.2014 • **Accepted/Published Online:** 18.08.2015 • **Printed:** 30.11.2015

Abstract: The photovoltaic power generation and active filter (PV-AF) system can realize photovoltaic grid-connected power regulation, and meanwhile it can also improve the power quality of power grid effectively. The four-leg grid-connected inverter has successfully been used in the three-phase four-wire system. In this paper, a three-dimensional space vector pulse width modulation (3D-SVPWM) method based on the ghγ coordinate system for a four-leg inverter has been proposed. As the switching vectors of the four-leg inverter are in the three-dimensional space, it is difficult to realize the complex modulation process. In order to simplify the modulation process, the reference vector is placed into ghγ coordinates in the proposed modulation strategy, and then the vectors are selected and the duration times are acquired directly by a group of intermediate variables, which could be obtained by linear transformation of the coordinates. As the intermediate variables are used, the modulation can be easily implemented by the proposed modulation strategy without excessive mathematical calculations. The simulation and experimental results all confirmed the validity and effectiveness of this strategy.

Key words: PV-AF system, ghγ coordinate, 3D-SVPWM, four-leg inverter

1. Introduction

Photovoltaic (PV) power generation systems, connected to the public grid through an inverter with suitable capacity, can relieve the energy crisis and reduce environmental pollution effectively [1]. In recent years, with the popularity of power electronics technologies, the problems of harmonics and three-phase unbalance in the three-phase four-wire system are becoming increasingly serious [2], which can be solved by the active filter (AF) [3–6]. The photovoltaic inverter is similar to the AFs in hardware structure and control method. PV power generation and AF (PV-AF) systems, unifying the two aspects, can solve the problem of low utilization ratio because of the change of the weather in the PV grid-connected inverter and improve the power quality of power grid effectively [7,8].

For the two-level inverter, the space vector pulse width modulation (SVPWM) strategy is generally adopted. Compared with other control methods, it excels in lower harmonic distortion of output voltage, easier digital implementation, higher utilization of DC voltage, etc. [9]. In the four-leg converter, as the sum of the three-phase voltage is not equal to zero, a 3D-SVPWM must be adopted. Currently, the conventional 3D-SVPWM algorithm is mainly based on the abc coordinate system [10,11] or $\alpha\beta\gamma$ coordinate system [12,13]. To realize the modulation function, both of these two types of algorithms are required to involve a lot of logic

*Correspondence: ariezjjz193@126.com

and arithmetic operations to determine the switching vectors adjacent to the reference vector and their duty cycles, which makes the 3D-SVPWM algorithm complex and difficult to apply.

In [14], a classification algorithm is used in the 3D-SVPWM algorithm to obtain intermediate variables, which are then used to determine the prism in which the reference vector is located as well as to calculate the duty cycles of the switching vectors. Although this method is much simpler than traditional ones [9–12], in order to determine the tetrahedron, another set of intermediate variables is required to be calculated. In addition, to calculate the duty cycles, linear transformation should be conducted for the intermediate variables obtained by the classification algorithm, which increases the computation load. In [15,16], the voltage vectors were placed into the gh coordinate system to complete the three-level SVPWM algorithm, and all the coordinates of switching vectors were integers. This paper proposes a new 3D-SVPWM strategy of a four-leg inverter based on the ghγ coordinate system based on the ideas of [14–16]. Different from the modulation algorithm in [14], the method proposed in this paper is to place the voltage vectors in the ghγ coordinate system and obtain the intermediate variables by the liner calculation of the reference vector in the ghγ coordinate system. The switching vectors adjacent to the reference vector are then determined based on the positive and negative values of intermediate variables, coupled with the duty cycles of the switching vectors. The effectiveness and feasibility of the algorithm will be proved by the simulation and experiments.

2. The distribution of four-leg inverter vectors in the ghγ coordinate system

The control block diagram of the PV-AF system is shown in Figure 1. The whole system is composed of a PV array, four-leg converter, four-wire load, and utility grid. The topology of the four-leg inverter is as shown in Figure 2, where a, b, c, and f are the 4 legs; v_a, v_b, v_c, and v_f respectively represent the output voltage of the 4 legs; and V_{dc} is the DC voltage.

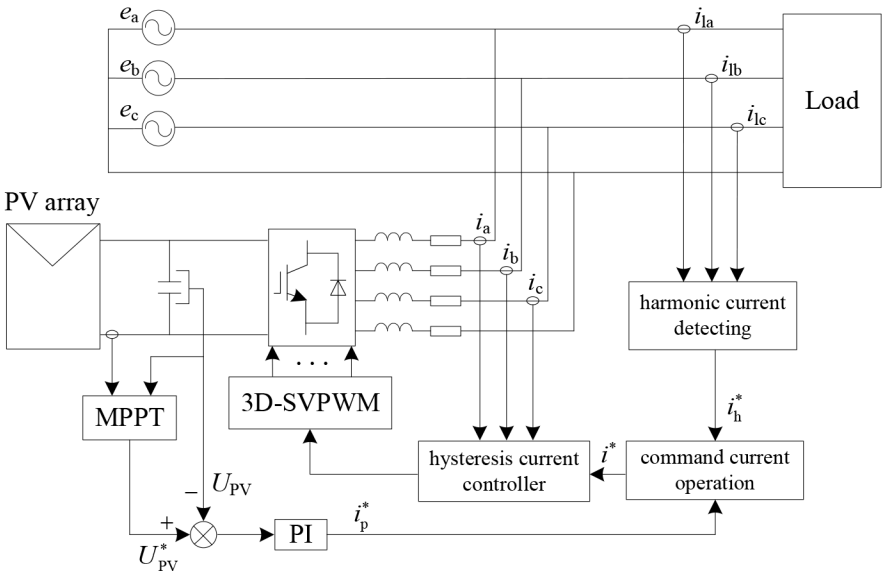

Figure 1. Control block diagram of the PV-AF system.

The switching vectors can be described by the ordered set [S_a, S_b, S_c, S_f,], where S_a = p denotes that the upper switch in phase a is closed, and S_a = n denotes that the bottom switch in phase a is closed. The same notation applies to phases b, c, and f.

As the projection of the switching vectors of the four-leg inverter is regular hexagon, it is feasible to create a 60° coordinate system in the plane. We set the 60° coordinate system as the gh coordinate system, take axis g to coincide with axis α in the $\alpha\beta$ coordinate system, carry out a counter-clockwise 60° rotation for the h axis, and take the γ axis as perpendicular to plane gh at the origin of the gh coordinates. Therefore, the ghγ coordinate system can be created.

In the two-level, three-phase, four-leg inverter, the 16 switching states form a hexagonal prism in the ghγ coordinate system that consists of 6 prisms, and each prism contains 8 switching vectors. The distribution of these vectors is as shown in Figure 3.

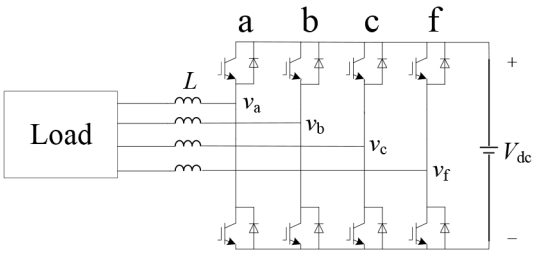

Figure 2. Four-leg inverter topology.

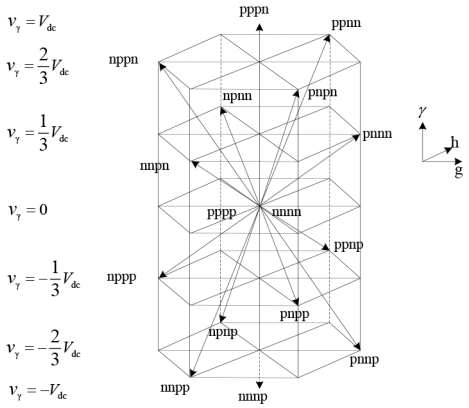

Figure 3. Switching vectors of a four-leg inverter.

The reference vector $\boldsymbol{V}_{\mathbf{ref}}$ is marked as (v_{af}, v_{bf}, v_{cf}) in the abc coordinates, and it is transformed as (v_g, v_h, v_γ) in the ghγ coordinates. The relationship between these 2 coordinate systems is shown in Eq. (1), and the results of the transformation are shown in Table 1.

$$\begin{bmatrix} v_g \\ v_h \\ v_\gamma \end{bmatrix} = \frac{2}{3}\begin{bmatrix} 1 & -1 & 0 \\ 0 & 1 & -1 \\ 1/2 & 1/2 & 1/2 \end{bmatrix}\begin{bmatrix} v_{af} \\ v_{bf} \\ v_{cf} \end{bmatrix} \tag{1}$$

3. 3D-SVPWM algorithm based on ghγ coordinate system

Intermediate variables x, y, z, s, q, and w can be obtained through v_g, v_h, and v_γ, and the linear transformation process is shown in Eq. (2). Intermediate variables can be utilized to determine the prism and the tetrahedron where the reference vector is located and calculate the duty cycles of the switching vectors.

$$\begin{cases} x(v_g,v_h,v_\gamma) = 3v_h \\ y(v_g,v_h,v_\gamma) = 2v_g+v_h+2v_\gamma \\ z(v_g,v_h,v_\gamma) = v_g-v_h-2v_\gamma \\ s(v_g,v_h,v_\gamma) = v_g+2v_h-2v_\gamma \\ q(v_g,v_h,v_\gamma) = 3v_g \\ w(v_g,v_h,v_\gamma) = 3(v_g+v_h) \end{cases} \tag{2}$$

Table 1. Switching combinations and converter voltages in ghγ coordinates.

	abcf	v_{af}/V_{dc}	v_{bf}/V_{dc}	v_{cf}/V_{dc}	$v_g/\frac{1}{3}V_{dc}$	$v_h/\frac{1}{3}V_{dc}$	$v_\gamma/\frac{1}{3}V_{dc}$
V_1	nnnn	0	0	0	0	0	0
V_2	nnpn	0	0	1	0	2	1
V_3	npnn	0	1	0	–2	2	1
V_4	nppn	0	1	1	–2	0	2
V_5	pnnn	1	0	0	2	0	1
V_6	pnpn	1	0	1	2	–2	2
V_7	ppnn	1	1	0	0	2	2
V_8	pppn	1	1	1	0	0	3
V_9	nnnp	–1	–1	–1	0	0	–3
V_{10}	nnpp	–1	–1	0	0	–2	–2
V_{11}	npnp	–1	0	–1	–2	2	–2
V_{12}	nppp	–1	0	0	–2	0	–1
V_{13}	pnnp	0	–1	–1	2	0	–2
V_{14}	pnpp	0	–1	0	2	–2	–1
V_{15}	ppnp	0	0	–1	0	2	–1
V_{16}	pppp	0	0	0	0	0	0

3.1. Determination of the prism

As can be seen from Figure 3, it is necessary to narrow the scope to a specific prism in order to determine the position of the reference vector in the hexagonal prism. The hexagonal prism is mapped onto plane gh, as shown in Figure 4, where $\boldsymbol{V}_{\mathbf{ref.gh}}$ is the projection of the reference vector $\boldsymbol{V}_{\mathbf{ref}}$ onto plane gh.

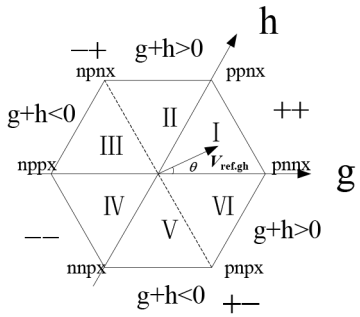

Figure 4. Projection of switching vectors in gh plane.

In Figure 4, the hexagon that is the projection of the switching vectors onto plane gh is divided into 6 triangles. Thus, the prism in which the reference vector is located can be determined through the v_g component and v_h component of the reference vector. The determination method is shown in Figure 5.

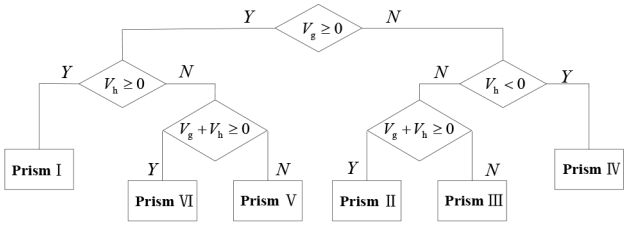

Figure 5. Determination method of the prism.

To simplify the determination process, when $q \geq 0$, let be $A = 1$, or otherwise A = 0; when $x \geq 0$, let be B = 0, or otherwise B = 0; when $w < 0$, let be C = 1, or otherwise C = 0. Also let $S = A + 2 \times B + 4 \times C$ be the relationship between S and the prism in which the reference vector lies, as shown in Table 2.

Table 2. Relationship between S and prisms.

Prism	**I**	**II**	**III**	**IV**	**V**	**VI**
S	3	2	6	4	5	1

4. Determination of the tetrahedron

After the determination of the prism in which the reference vector is located, it needs to be redivided due to the fact that each of the prisms contains 6 nonzero vectors and 2 zero vectors. The prism can be divided into 4 tetrahedrons and each tetrahedron consists of 3 nonzero vectors and 2 zero vectors. Only by determining the tetrahedron in which the reference vector is located can switching vectors be chosen to synthesize the reference vector.

Taking Prism I as an example, the distribution of its switching vectors is shown in Figure 6. It can be seen that the prism is divided into 4 tetrahedrons by boundary planes A, B, C, D, and E, and each tetrahedron is composed of 3 boundary planes. The boundary planes can be used to identify the tetrahedron in which the reference vector lies, and thus the adjacent switching vectors are obtained.

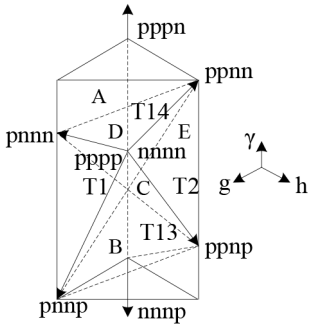

Figure 6. Prism I and four tetrahedrons in Prism I.

The equations of planes A, B, C, D, and E can be obtained based on the coordinates of the switching vectors, as shown in Eq. (3). By substituting the coordinates of the reference vector into Eq. (2), we can see that: 1) when the reference vector is in the range of T1, $x > 0$, $y > 0$, and $z > 0$; 2) when it is in the range of T2, $z < 0, s > 0$, and $q > 0$; 3) when it is in the range of T13, $x > 0$, $y < 0$, and $q > 0$; 4) when it is in the range of T14, $x > 0$, $s < 0$, and $q > 0$.

$$\begin{cases} \text{A} : v_h = 0 \\ \text{B} : 2v_g + v_h + 2v_\gamma = 0 \\ \text{C} : v_g - v_h - 2v_\gamma = 0 \\ \text{D} : v_g + 2v_h - 2v_\gamma = 0 \\ \text{E} : v_g = 0 \end{cases} \tag{3}$$

Similarly, the tetrahedron in which the reference vector is located can be determined when it is within other prisms, and the determining process is shown in Figure 7.

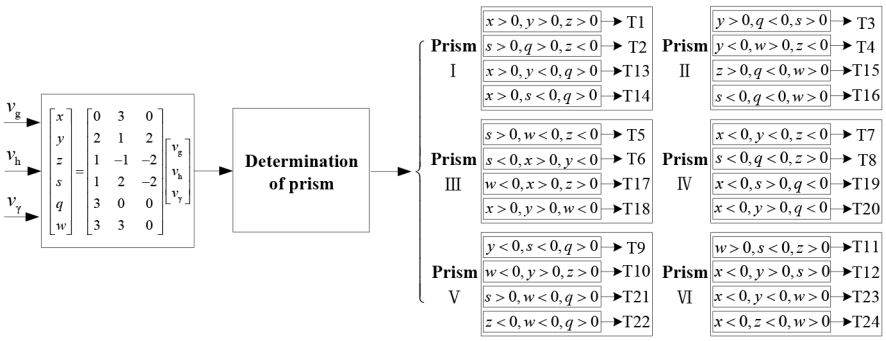

Figure 7. Determination method of the reference vector location.

4.1. Calculation of the duration time of the adjacent switching vectors

Taking the reference vector $\boldsymbol{V}_{\mathbf{ref}}$ in Tetrahedron T1 as an example, the available switching vectors are $\boldsymbol{V}_{\mathbf{d1}}$ = pnnn, $\boldsymbol{V}_{\mathbf{d2}}$ = pnnp, $\boldsymbol{V}_{\mathbf{d3}}$ = ppnp, and $\boldsymbol{V}_{\mathbf{d0}}$ = [pppp, nnnn]. Assuming the duration times are t_1, t_2, t_3, and t_0, respectively, the DC voltage is V_{dc}, and the SVPWM specified switching cycle is T_s. According to the volt-second balance principle, the corresponding duration times of the switching vectors are given by:

$$\mathbf{V_{ref}}T_s = \mathbf{V_{d1}}t_1 + \mathbf{V_{d2}}t_2 + \mathbf{V_{d3}}t_3 + \mathbf{V_{d0}}t_0, \tag{4}$$

$$\begin{bmatrix} t_1 \\ t_2 \\ t_3 \end{bmatrix} = \frac{T_s}{2V_{dc}} \begin{bmatrix} 2 & 1 & 2 \\ 1 & -1 & -2 \\ 0 & 0 & 3 \end{bmatrix} \begin{bmatrix} v_g \\ v_h \\ v_\gamma \end{bmatrix} \quad , \tag{5}$$

$$t_0 = T_s - t_1 - t_2 - t_3 \quad . \tag{6}$$

Combining Eqs. (2) and (5), it can be seen that

$$\begin{cases} t_1 = \frac{y}{2V_{dc}}T_s \\ t_2 = \frac{z}{2V_{dc}}T_s \\ t_3 = \frac{x}{2V_{dc}}T_s \end{cases} . \tag{7}$$

The duration times can be expressed by the intermediate variables in Eq. (7). Similarly, the duty cycles of the adjacent switching vectors can be obtained when the reference vector is located in other tetrahedrons. Table 3 lists the corresponding duration times of the switching vectors when the reference vector is located in the tetrahedron of the Prism I, where $a = T_s/2V_{dc}$. It can be seen that duration times could be represented by the intermediate variables, so it is unnecessary to calculate the duration times.

Table 3. Switching durations of adjacent switching vectors in Prism I.

Tetrahedron	$\boldsymbol{V_1}$	$\boldsymbol{V_2}$	$\boldsymbol{V_3}$	t_1/a	t_2/a	t_3/a
T1	pnnn	pnnp	ppnp	y	z	x
T2	pnnn	ppnn	ppnp	q	$-z$	s
T13	nnnp	pnnp	ppnp	$-y$	q	x
T14	pnnn	ppnn	pppn	q	x	$-s$

4.2. Switching sequence

Since the duration times of the space vectors are already determined, the switching sequence should be defined in the next moment. The switching sequence will influence the harmonic content of converter output and switching loss [12,13].

In order to minimize the harmonics produced by the converter, in this work, the sequence uses both zero vectors, as shown in Figure 8. Figure 8 shows the sequence for Tetrahedron T1 and there will be a similar sequence if the reference vector is located in other tetrahedrons.

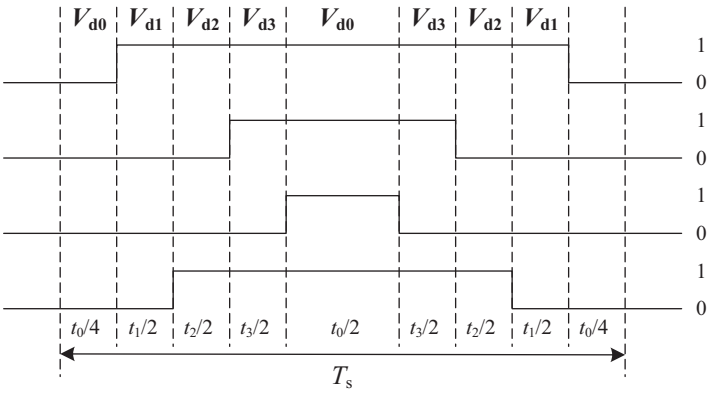

Figure 8. Switching sequence for Tetrahedron T1 space vectors.

In the modulation algorithm based on the abc coordinates or $\alpha\beta\gamma$ coordinates, in order to judge the place where the reference vector is located and calculate the duration times of the switching vectors, many variables need to be involved. Compared with the two kinds of classification algorithm, the proposed modulation algorithm is implemented among 6 intermediate variables without calculating other variables, which can reduce the calculation load. Furthermore, as the voltage vectors are in the ghγ coordinate system, there is no need to calculate the square root in the process of obtaining the intermediate variables, which can improve the accuracy of the operation and reduce the complexity of the arithmetic operation. As a result, the microprocessors are able to allow more time to calculate other modules of PV-AF.

5. Simulation and experimental results

The new 3D-SVPWM algorithm is simulated in MATLAB/Simulink software. The main circuit is the two-level, four-leg inverter and the parameters of the simulation are shown in Table 4.

Table 4. Parameters of the inverter simulation.

Load	R= 7 Ω, L= 5 mH
DC voltage: V_{dc}	57 V
Line frequency	50 Hz
Amplitude of the AC voltage	20 V
Carrier frequency of the system	5 kHz

The reference voltages are set as

$$\begin{cases} u_{refa} = 20\sin(\omega t) \\ u_{refb} = 20\sin(\omega t - 120^\circ) \\ u_{refc} = 20\sin(\omega t + 120^\circ) \end{cases}. \tag{8}$$

The simulation results under the reference voltage are as shown in Figure 9. Figure 9a shows the modulation wave of the a-phase; after the filtering of the low-pass filter with the cutoff frequency of 400 Hz, the output voltage waveform of the inverter is as shown in Figure 9b; Figure 9c shows the a-phase current waveform; and by conducting fast Fourier transform (FFT) analysis of the a-phase voltage and a-phase current, it can be seen that the total harmonic distortion (THD) rate of the a-phase voltage is 0.89%, the peak of the a-phase current is 2.79 A, and the THD rate is 2.37%, for which the a-phase current spectrum is as shown in Figure 9d.

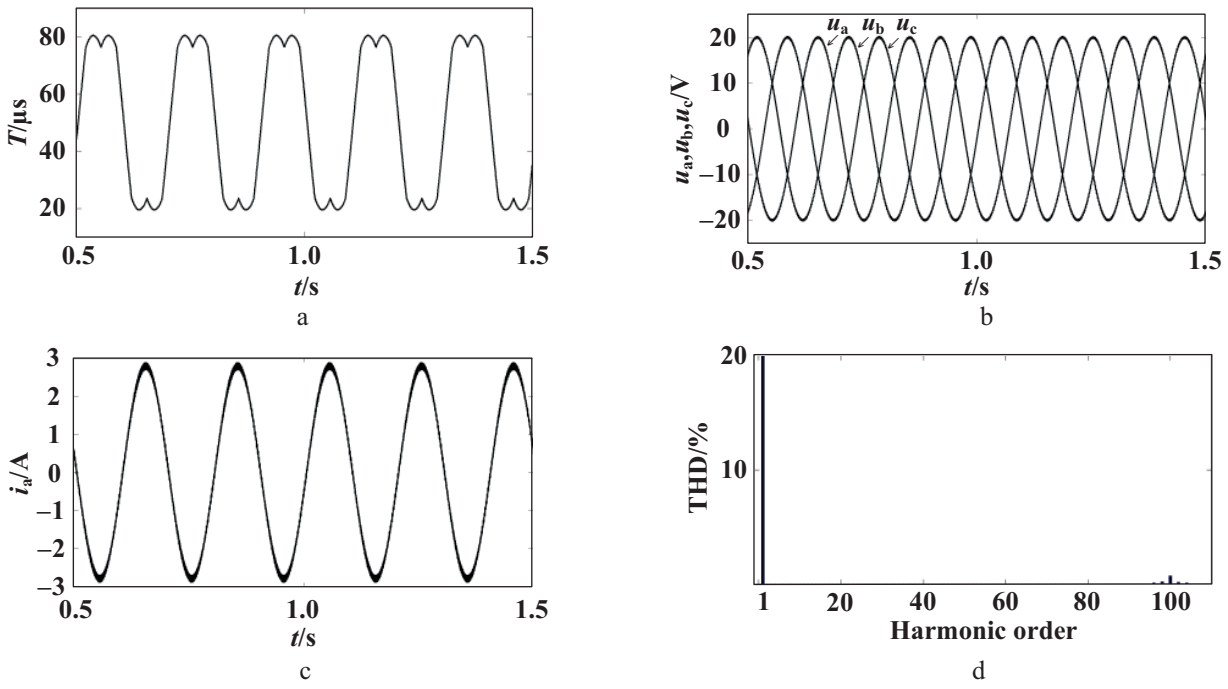

Figure 9. Main waveforms with symmetrical reference voltage without distortion: a) modulation wave of a-phase, b) three-phase voltage, c) a-phase current, d) a-phase current spectrum.

Figure 9 shows that when the reference voltage is symmetric, the three-phase voltage output of the inverter when using the new 3D-SVPWM algorithm matches the reference voltage, and low THD of the voltage and current is achieved.

The reference voltage are set as

$$\begin{cases} u_{refa} = 20\sin(\omega t) + 4\sin(5\omega t) \\ u_{refb} = 20\sin(\omega t - 120^\circ) \\ u_{refc} = 20\sin(\omega t + 120^\circ) \end{cases}. \tag{9}$$

Under this reference voltage, the output waveform of the three-phase voltage of the inverter is as shown in Figure 10a, and the waveform of the a-phase output current is as shown in Figure 10b. Conducting FFT analysis of the three-phase voltage and a-phase currents, respectively, the results indicate that the THD rates of the a, b, and c phase voltages are respectively 19.72%, 0.88%, and 0.88%, and the THD rate of the a-phase current is 10.66%; the spectrums of the a-phase voltage and a-phase current are as shown in Figures 10c and 10d. Figure 10e shows the modulation wave of the a-phase.

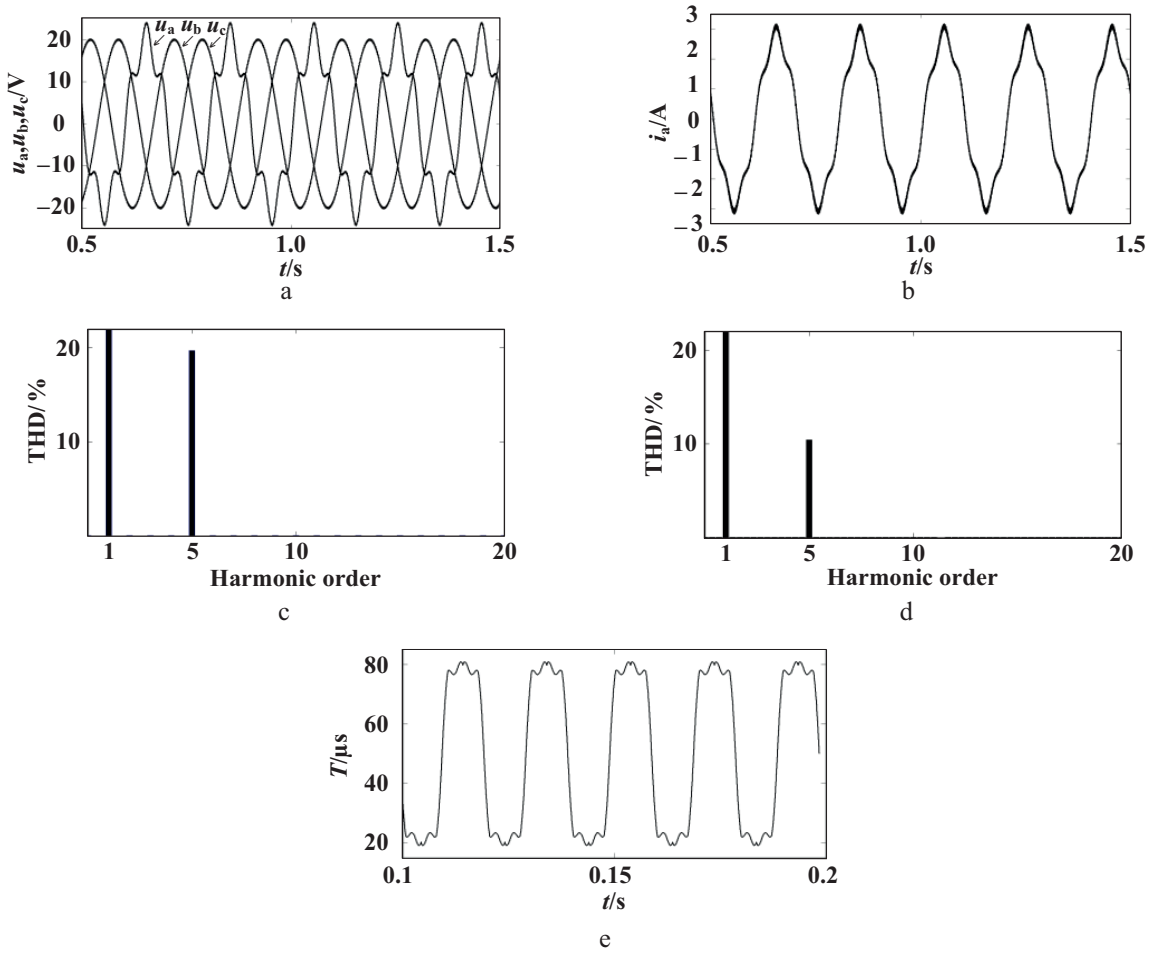

Figure 10. Main waveforms with phase-a reference voltage including the fifth harmonic: a) three-phase voltage, b) a-phase current, c) a-phase voltage spectrum, d) a-phase current spectrum, e) modulation wave of a-phase.

Figure 10 shows that when the reference voltage contains harmonic content, the output voltage modulated by the new 3D-SVPWM algorithm can track the reference voltage.

The above simulation waveforms verify the correctness of the new 3D-SVPWM algorithm. Whether or not distortion of the three-phase reference voltage exists, the output voltage of the inverter matches the reference voltage.

For the PV-AF system, the simulation parameters are shown in Table 5. Suppose that the output voltage of the PV array is invariable and the load of the system is the three-phase uncontrolled rectifier parallel three-phase resistance. The instantaneous reference current for compensation is detected by the method based on the instantaneous reactive power theory, and the proposed 3D-SVPWM method is used to modulate the four-leg inverter. The supply current and the supply voltage of the a-phase are shown in Figure 11a. The a-phase current reference and the a-phase output current waveform of the PV-AF system are shown in Figures 11b and 11c, respectively. It can be seen that the output current could match the reference signal, which proves that the proposed 3D-SVPWM method is validated and easy to implement.

Table 5. Parameters of PV-AF simulation model.

Parameters	Value
Output voltage of the PV array, V	650
AC voltage, V	110
DC voltage, V	420
Inlet inductance of the PV-AF system, mH	3
Equivalent resistance of the inlet inductance, Ω	0.1
Load of the three-phase uncontrolled rectifier, Ω	75
Three-phase resistance, Ω	50

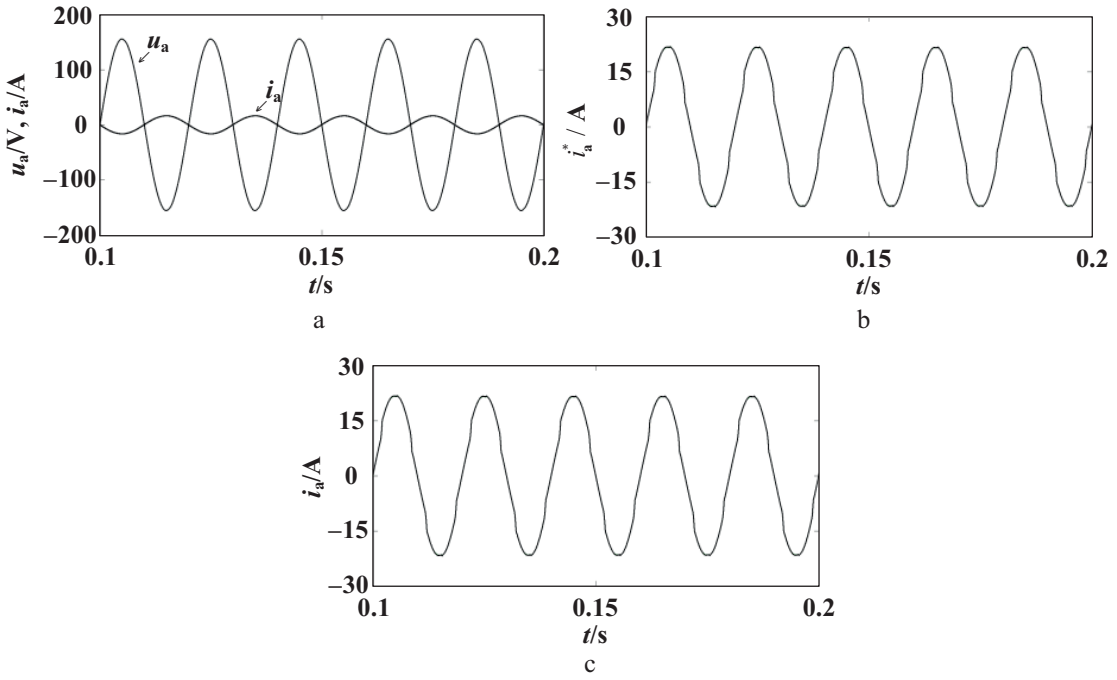

Figure 11. Main waveforms in the PV-AF system: a) supply current and voltage waveform of a-phase, b) instruction signal of a-phase current, c) a-phase output current waveform of the PV-AF system.

When the reference voltage is as in Eq. (8), the waveform of a-phase modulation output by the D/A is as shown in Figure 12a, which is saddle wave and is consistent with Figure 9a; Figures 12b and 12c respectively show the three-phase current waveform and the spectrum of the a-phase current. These figures indicate that the peak of three-phase current is 2.8 A, and the spectral analysis of the a-phase current shows that the THD rate is 1.8%. The a-phase current waveform contains a small number of odd harmonics, which are mainly caused by the dead-time effect of PWM.

If the reference voltage is unbalanced, as shown in Eq. (9), the experimental results are as shown in Figure 13a, which is consistent with Figure 10. The a-phase current waveform with 1.979A RMS and the spectrum of the a-phase current with 10.6% THD are shown in Figures 13b and 13c, respectively. These experimental results further show the correctness of the proposed 3D-SVPWM algorithm and the feasibility in practical applications.

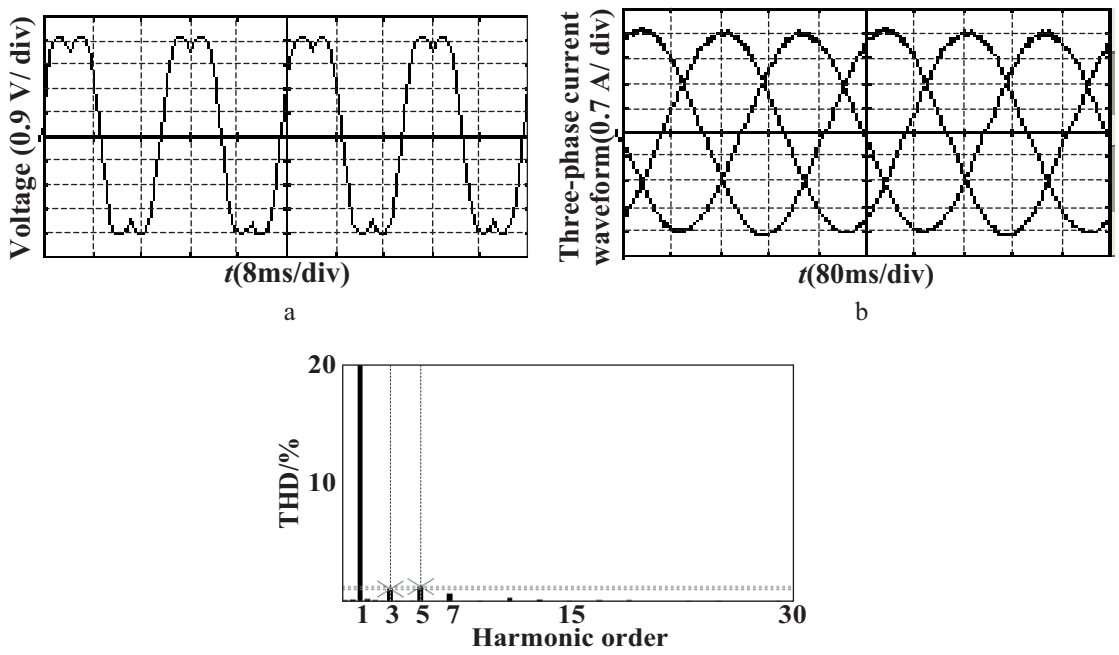

Figure 12. Main experimental waveforms with symmetrical reference voltage without distortion: a) modulation wave of a-phase, b) three-phase current, c) a-phase current spectrum.

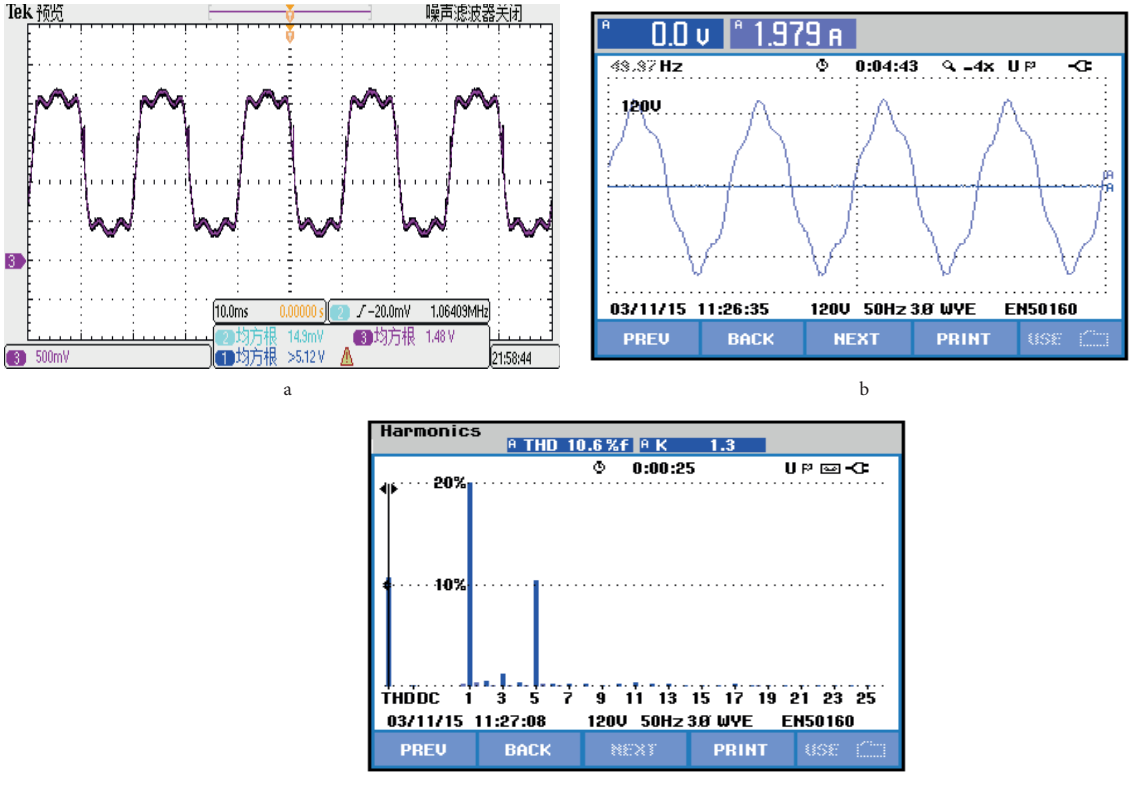

Figure 13. Main experimental waveforms with phase-a reference voltage including the fifth harmonic: a) modulation wave of a-phase, b) a-phase current, c) a-phase current spectrum.

6. Conclusion

This paper, with the four-leg inverter as the object of study, has proposed a new three-dimensional vector modulation strategy based on the ghγ coordinate system targeting the problems of large computations and complex processes of the conventional modulation algorithm in abc coordinates and $\alpha\beta\gamma$ coordinates, which is shown as follows: 1) the prism where the reference vector is located is determined by the relationship between the projection of the reference vector on plane gh and the g and h axes; 2) a detailed analysis of the relationship between the reference vector and the five boundary planes within each prism in ghγ coordinates is carried out, which is used as a basis for determining the tetrahedron where the reference vector lies; 3) comparing the duration time of the switching vectors with the intermediate variables, the duty cycles can be represented by the intermediate variables. The determination process of the switching vectors is simplified in the proposed algorithm, and it is not necessary to calculate the switching durations. Thus, the computational work of the modulation algorithm is reduced greatly compared with the classification algorithm. Simulation and experimental results both verify the correctness and effectiveness of the algorithm.

Acknowledgment

This work was supported by National Natural Science Foundation of China (51407184).

References

[1] Blaabjerg F, Teodorescu R, Liserre M, Timbus AV. Overview of control and grid synchronization for distributed power generation systems. IEEE T Ind Electron 2006; 53: 1398–1409.

[2] Dang PP, Ellinger T, Petzoldt J. Dynamic interaction analysis of APF systems. IEEE T Ind Electron 2014; 61: 4467–4473.

[3] Abdelkrim T, Berkouk EM, Benamrane K, Benslimane T. Study and control of 5-level PWM rectifier-5-level NPC active power filter cascade using feedback control and redundant vectors. Turk J Electr Eng Co 2012; 20: 655–677.

[4] Rahmani S, Hamadi A, Al-Haddad K, Dessaint LA. A combination of shunt hybrid power filter and thyristor-controlled reactor for power quality. IEEE T Ind Electron 2014; 61: 2152–2164.

[5] Vodyakho O, Mi CC. Three-level inverter-based shunt active power filter in three-phase three-wire and four-wire systems. IEEE T Power Electron 2009; 24: 1350–1363.

[6] Vodyakho O, Kim T. Shunt active filter based on three-level inverter for three-phase four-wire systems. IET Power Electron 2009; 2: 216–226.

[7] Singh M, Khadkikar V, Chandra A, Varma RK. Grid interconnection of renewable energy sources at the distribution level with power-quality improvement features. IEEE T Power Deliver 2011; 26: 307–315.

[8] Hosseini SH, Danyali S, Yazdanpanah Goharrizi Y. Three phase four-wire grid-connected PV power supply with accurate MPPT for unbalanced nonlinear load compensation. In: 2009 International Symposium Industrial Electronics; 5–8 July 2009; Seoul, South Korea. New York, NY, USA: IEEE. pp. 1099–1104.

[9] Li XS, Deng ZQ, Chen ZD, Fei QZ. Analysis and simplification of three-dimensional space vector PWM for three-phase four-leg Inverters. IEEE T Ind Electron 2011; 58: 450–464.

[10] Monroy Morales JL, Hernandez Angeles M, Vargas FHV. A digital control for a three-dimensional SV-PWM multilevel converter. In: IEEE International Autumn Meeting on Power, Electronics and Computing; 5–7 November 2014; Ixtapa, Mexico. New York, NY, USA: IEEE. pp. 1–6.

[11] Franquelo LG, Prats MAM, Portillo RC, Galvan JIL, Perales MA, Carrasco JM, Díez EG, Jiménez JLM. Three-dimensional space-vector modulation algorithm for four-leg multilevel converters using abc coordinates. IEEE T Ind Electron 2006; 53: 458–466.

[12] Liu X, Xie YX, Wang Y. A simplified 3D-SVPWM algorithm for three-phase four-wire shunt active power filter. In: 17th International Conference on Electrical Machines and Systems; 22–25 October 2014; Hangzhou, China. New York, NY, USA: IEEE. pp. 1457–1462.

[13] Zhang R, Prasad VH, Boroyevich D, Lee FC. Three-dimensional space vector modulation for four-leg voltage-source converters. IEEE T Power Electron 2002; 17: 314–326.

[14] Zhou J, Wu X, Jiang ZY, Zhang Y, Wu XJ. A novel 3D-SVPWM algorithm for four-leg converter. Chin Soc Elec Eng 2011; 25: 1–8 (in Chinese with abstract in English).

[15] Celanovic N, Boroyevich D. A fast space-vector modulation algorithm for multilevel three-phase converters. IEEE T Ind Appl 2001; 37: 637–641.

[16] Zheng JY, Shen ZL, Mei J, Wang LF. An improved neutral-point voltage balancing algorithm for the NPC three-level inverter based on virtual space vector PWM. In: Electrical and Control Engineering; 25–27 June 2010; Wuhan, China. New York, NY, USA: IEEE. pp. 3283–3287.